Masters Theses   Graduate Research and Creative Practice

8-2019

Methods of Estimating Foot and Ankle Power in Takeoff Phase of Standing Vertical Jump

Kundan Joshi
Grand Valley State University

Methods of Estimating Foot and Ankle Power in Takeoff Phase of Standing Vertical Jump

Kundan Joshi

A Thesis Submitted to the Graduate Faculty of

GRAND VALLEY STATE UNIVERSITY

In

Partial Fulfillment of the Requirements

For the Degree of

Master of Science in Engineering, Biomedical Engineering

School of Engineering

August 2019

Thesis Approval Form
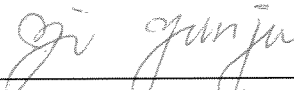
GRAND VALLEY STATE UNIVERSITY

The signatories of the committee members below indicate that they have read and approved the thesis of Kundan Joshi in partial fulfillment of the requirements for the degree of Master of Science in Engineering.

_____   7-16-2019
Dr. Blake Ashby, Thesis committee chair   Date
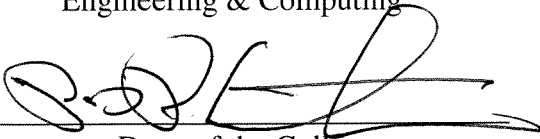
_____   7-16-2019
Dr. Gordon Alderink, Committee member   Date

_____   7-17-2019
Dr. Yunju Lee, Committee member   Date

Accepted and approved on behalf of the   Accepted and approved on behalf of the
Padnos College of   Graduate Faculty
Engineering & Computing
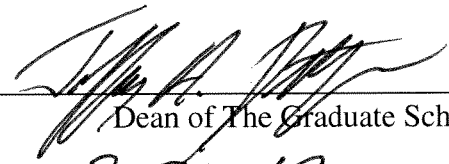
_____   _____
Dean of the College   Dean of The Graduate School

7/18/2017   7-30-19
_____   _____
Date   Date

Acknowledgements:

I would like to thank all my thesis committee members for their time and effort into the completion of my thesis. I have to express my most sincere thanks to my advisor, Dr. Blake Ashby, for his guidance and contributions through all the hurdles that I encountered both through my thesis and my master's degree program. His knowledge and expertise in the field of movement biomechanics has immensely helped in the completion of this work. I also want to thank Dr. Gordon Alderink and the staff of Biomechanics and Motor Performance Laboratory in assisting with data collection sessions. Dr. Alderink's expertise and experience in motion capture was indeed instrumental for this work. I would also like to thank Dr. Yunju Lee, for her big-picture perspective and positive suggestions. I have to also thank the staff of Statistical Consulting Center of GVSU for their efforts with the statistical analyses. Finally, I would like to thank the participants who volunteered their time and effort, as well as my family for providing me constant support through all this time.

Abstract:

Experimental motion capture studies have commonly considered the foot as a single rigid body. However, the presence of internal joints as well as soft-tissue interactions inside the foot demonstrate that the foot is in fact not rigid. Various methods have been applied to study the deviations of the foot from rigid body mechanics, such as developing multi-segment foot models or employing compensation strategies for the rigid foot model. However, no study has compared these compensation strategies with multi-segment models in any movement such as gait or jumping. This study compared two main compensation strategies (distal foot power and power balance technique) as well as a two-segment foot model to study the power and work of the foot and the ankle in the takeoff phase of the standing vertical jump. Physically active participants (ages 20 – 26 years) performed several standing vertical jumps from a specific starting position spanning two adjacent force platforms such that the ground reaction forces (GRF) acting on the foot were divided at the metatarsophalangeal (MTP) joints.

The results of the study showed that the three methods for calculating work internal to the foot were significantly different from each other. Distal foot work was -4.0 ± 1.0 J, foot work from power balance was 1.8 ± 1.1 J, and MTP joint work was 5.1 ± 0.5 J. Distal foot power showed a power absorption peak up to 111 W at around 0.1 seconds before takeoff, immediately followed by a peak power generation of 102 W. Foot power imbalance followed a similar pattern with a 31 W power absorption peak immediately followed by peak power generation of 135 W. There was minimal power absorbed at the MTP joints (a minor 7 W peak absorption) shortly after movement initiation, but apart from that, the MTP joints only generated power reaching a peak of 127 W. The results for ankle power and work did not show clinically significant difference between using the rigid foot model (58.3 ± 3.1 J) and multi-segment foot model (59.9 ± 3.4 J),

even with the substantial power generation at the MTP joints. The likely cause for the similar ankle work values was that the anatomical reference frames for the entire rigid foot and for the rear foot were defined using the same markers (on the calcaneus, first and fifth metatarsal head). When the marker set defining the anatomical reference frame of the rear-foot were changed to ones on the calcaneus, navicular, and cuboid bones, the rigid foot model overestimated the ankle power in comparison to the multi-segment foot. The possible reason for this was that the new markers were all on the more rigid hind-foot, which led to the rear-foot being modeled as equivalent to a more rigid hind-foot and a massless midfoot.

The results suggest that MTP joints are only one source of the foot power and that comparison between distal foot power and power balance technique should be further explored in jumping and other movements. Improvements in the understanding of foot and ankle mechanics in standing vertical jump might also be obtained by implementing a foot model with more than two segments. This would require a better way of distributing the ground reaction kinetics between the foot segments because the adjacent force platform method would not be practicable.

Table of Contents:

List of Figures:

List of Tables:

1   Introduction:

Experimental motion capture studies of human body motions such as gait, running, and jumping

commonly model the body as a series of rigid links connected by ideal joints. The rigid body

assumption simplifies various analyses. However, this assumption is better for some segments

like the thigh and shank than it is for other segments like the foot and trunk. How good the rigid

body assumption for a given segment is can be quantified by the difference between the net

power into and out of the segment and the time rate of change of total segmental energy. For a

rigid body, this difference theoretically should be zero or practically close to zero. Hence, any

deviations from a rigid body model are reflected in this difference in power.

In inverse dynamics analyses of the foot using rigid body assumptions, this difference in power

term is usually non-zero. The human foot indeed is not rigid as it is comprised of 26 joints:

subtalar, talonavicular, calcaneal-cuboid, as well as joints involving the cuneiform, metatarsal,

and phalangeal bones. There is movement about these internal foot joints, which along with other

internal deformations could be the reason for the power imbalance at the foot. Mathematical

representations of this deformation power have been developed with the concept of distal foot

power (Siegel et al., 1996) and by the power balance technique (Robertson and Winter, 1980).

Distal foot power considers the foot as a rigid body as it contacts the ground. Using rigid body

kinematics equations, the velocity at the center of pressure between the foot and ground is

calculated to be non-zero. This non-zero distal foot velocity results in non-zero distal foot power.

Using the power balance technique (Robertson and Winter, 1980), all active and passive power

transfer terms into and out of the segment are calculated and compared with the segmental rate of

energy change. The difference between the two is the power imbalance term (ΔP). To achieve

better power balance, the 3DOF (degrees of freedom) approach was modified to a 6DOF

approach (Buczek et al., 1994) considering both translational and rotational motion at the joints. Better estimates of ankle and foot power in gait were obtained using a 6DOF model (Zelik et al., 2015). Multiple studies (McGibbon and Krebs, 1998; Takahashi et al., 2012; Takahashi and Stanhope, 2013; Zelik et al., 2018) have used the concept of the distal foot power, whereas the power balance technique has not been explored as much.

Another approach that may be able to account for the non-rigid nature of the foot is to model it with multiple segments. Commonly used multi-segment foot models include the Leardini (Leardini et al., 1999) and the Oxford Foot Models (Carson et al., 2001). However, most of the multi-segment foot studies only performed kinematic analysis, since a full kinetic analysis would require partitioning the ground reaction force (GRF) acting on each of the foot segments. MacWilliams et al. (2003) conducted a comprehensive kinematic and kinetics analysis by using a pressure platform to divide the GRF into sub-area shear and normal forces. Their main assumption was that the shear forces for foot segments could be divided in the same proportion as the normal forces were divided. In contrast to a pressure platform approach, Bruening et al. (2010, 2012b) developed a multiple force platform approach using two adjacent force platforms to separately measure GRF components in adjacent foot segments. Recent research has shown that the two-force platform approach is the gold standard when compared to the proportionality assumption method (Bruening and Takahashi, 2018). Analysis using multi-segment gait foot models have highlighted the important role of inter-foot joint contributions to power calculations that a rigid body model cannot consider.

In comparison to gait analysis, minimal research has been conducted on jumping studies using a multi-segment foot. Stefanyshyn and Nigg (1998) in their analysis of a two-segment foot in running long and running vertical jumps used a pressure platform approach. They highlighted the

12

role of joints internal to the foot in jumping. No study has used a multi-segment foot to

investigate the standing vertical jump. The standing vertical jump is a common movement

present in sports such as football, basketball, and volleyball. Most of the standing vertical jump

research has focused on hip, knee, and ankle joint dynamics (Robertson and Fleming, 1987;

Nagano et al., 1998; Vanrenterghem et al., 2004). No research has used techniques such as distal

foot power and power balance to study power contributions internal to the foot in jumping.

Understanding internal power contributions may help researchers to better analyze jumping

performance, decrease injury risks, and improve sport training and rehabilitation.

The primary aims of the current study were to perform inverse dynamic analyses of the takeoff

phase of standing vertical jumps and analyze power and work in the foot and the ankle using the

approaches described in.
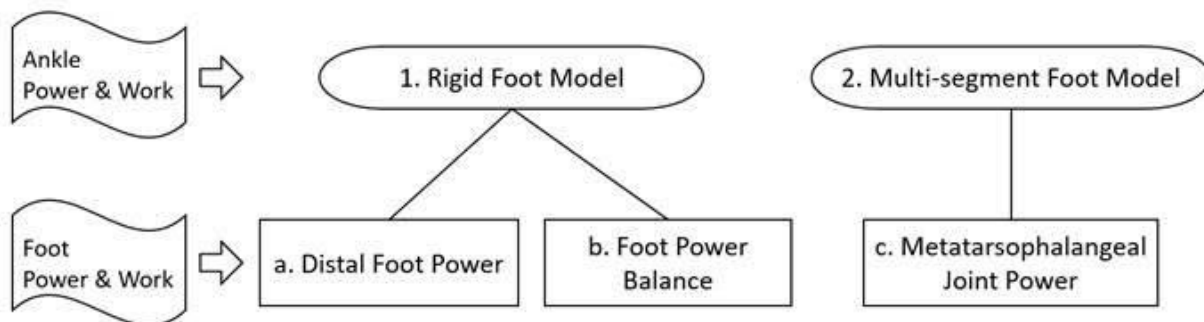
Figure 1 Comparison Parameters and Approaches within aims of the study

2 Literature Review:

2.1 Estimating Foot Power with a Single Rigid Segment:

The rigid body assumption for the foot does not account for power generation and absorption internal to the foot leading to power imbalance. To compensate for the internal power terms, different strategies for estimating the power and work performed within the foot have been developed. One strategy introduced by Siegel et al. (1996) is referred to as distal foot power. The formulation for calculating distal foot power is shown in Eqn. 1. With the inclusion of the distal foot power and the concept of 3DOF joints, the results indicated a closer proximity of segmental power and rate of change of segmental energy graphs in comparison to foot power using 2DOF joints and zero distal power terms.

$$P_{dfp} = \boldsymbol{F}_{GRF} \cdot \boldsymbol{v}_d + \boldsymbol{M}_{free} \cdot \boldsymbol{\omega}_f \qquad \text{Eqn. 1}$$

Where, $\boldsymbol{F}_{GRF}$ is the ground reaction force acting on the foot at the center of pressure (COP), $\boldsymbol{M}_{free}$ is the free moment acting on the foot, $\boldsymbol{\omega}_f$ is the angular velocity of the foot, and $\boldsymbol{v}_d$ is the distal foot velocity given by Eqn. 2.

$$\boldsymbol{v}_d = \boldsymbol{v}_G + \boldsymbol{\omega}_f \times \boldsymbol{r}_d \qquad \text{Eqn. 2}$$

Where, $\boldsymbol{v}_G$ is the velocity of the mass center of the foot, $\boldsymbol{r}_d$ is the position vector from the foot's mass center to the COP.

Numerous studies have subsequently applied and extended the concept of distal foot power. McGibbon and Krebs (1998) compared four different methods to study power imbalance of the foot. Three methods used the concept of distal foot velocity and power whereas the fourth method used the power contribution of the motion of segment endpoints relative to the mass center, terming it radial velocity. When radial velocity was set to zero for the foot (i.e., no length

14

changes were allowed for the foot) and distal foot velocity was included, power imbalance was low. When the term was set to non-zero, allowing for length changes, power imbalance was high for the foot.

The concept of 6DOF power analysis was introduced by Buczek et al. (1994) before the distal foot power concept. Basically, a joint with 6DOF allows rotational and translational motion for all three orthogonal directions. The concepts of 6DOF and distal foot power was combined in various studies for different purposes. One such study (Zelik et al., 2015) tried to improve the total body work estimates obtained using a conventional 3DOF approach by applying 6DOF analysis on hip, knee, and ankle joints and including distal foot power. The results suggested that 6DOF analysis improved the foot power estimates in the phases of gait where energy was usually positive (rebound and toe-off).

Other studies looked at improving prosthetic designs for amputees (Takahashi et al., 2012; Takahashi and Stanhope, 2013). Lower limb prosthetic designs have increasingly progressed to compensate for missing ankle joint contributions. Takahashi et al. (2012) comapred a lower limb containing shank and foot separated by an anatomical ankle joint, versus a below-knee prosthetic limb with proximal rigid component analogous to anatomical shank and deformable distal component. The sum of ankle and distal foot power for the anatomical model was very close to the distal segment power of the prosthetic limb model. These results indicated a novel way of utilizing distal segment power to study kinetics of various below-knee prosthetics. Other modern prosthetics use motors and actuators to provide active energy recoil. According to the Takahashi and Stanhope (2013) study, these active prosthetics need to compensate for the over-estimation of ankle-foot power by studies employing rigid body models due to soft tissue deformations in the foot. Hence, this study focused on the natural ankle-foot system and compared the distal foot

power and combined ankle-foot power at different walking speeds. Takahashi and Stanhope (2013) also calculated the work-ratio of the ankle joint (ratio of total positive work to absolute value of total negative work), which included the distal foot power terms. On average, the ratio was found to be 0.87 for normal walking speed. A value of 1.0 for the ankle was considered the maximum functional limit for a passive dynamic prosthetic. The results suggested that a prosthetic foot consisting of elastic materials can potentially replicate the power profiles of the ankle as well as compensate for power terms distal to the ankle.

Zelik et al. (2018) reviewed different methods for studying ankle and foot power. One of the most notable differences was seen in how the concept of ankle + distal foot power was applied versus a slight modification of it by calculating distal calcaneus power instead. The distal calcaneus power method considered the motion of the shank relative to the rigid calcaneus by studying the kinetics of the Ankle Joint Complex (AJC). AJC represented the combination of talocrural and subtalar joints. In doing so, calcaneus was classified as one rigid segment and the contributions from rest of the foot were included in distal calcaneus power. Power profiles for the combined ankle and foot for both methods showed nearly identical results. However, individual results of AJC versus ankle power as well as distal calcaneus versus distal foot power showed contrasting results. While distal calcaneus power profiles showed energy storage and return in the foot during late stance, distal foot power profiles only showed energy dissipation.

A different approach for estimating the power absorbed and generated in the foot is the segmental power balance technique (Robertson and Winter, 1980; Winter, 1996). The basis of this approach is that the net active and passive power flow into and out of a segment should equal the time rate of change of segmental energy. If they are not equal, then there is a power imbalance. This power imbalance is a result of power absorption and/or generation within the

segment. For the thigh and shank, this difference is typically close to zero, meaning that the rigid body assumption is good for those segments. However, for the foot, the power imbalance is often non-negligible. Robertson and Winter (1980) showed that power balance of the foot was achieved in mid-stance and early push-off phases of gait, but that power imbalance was high in early stance and late push-off phases. This power imbalance in the foot during gait was further investigated several years later (Winter, 1996). In early stance, a fraction of the power transferred into the foot through the ankle was transferred to the forefoot fat pad. Subsequently, in late stance, a fraction of the power generated at the ankle was due to elastic recovery of the previously stored energy in the viscoelastic tissues in the foot and/or generated at the metatarsophalangeal joints. This power imbalance in the foot indicates a deviation from the rigid body mechanics of the segment.

2.2   Multi-segment Foot Kinematics and Kinetics:

Several researchers have developed multi-segment models of the foot. One of the earliest multi-segment foot models was developed with eight segments and eight 1-DOF hinge joints (Scott and Winter, 1993). The complexity of the model was high given that springs and dampers were used to model soft-tissue compression. A four-segment foot model was then developed (Leardini et al., 1999) to standardize anatomical frames for the segments. Carson et al. (2001) developed a three-segment foot model with 6DOF joints between segments, which is popularly known as the Oxford Foot Model. The Leardini and Oxford Foot models are the most commonly adopted foot models and many subsequent studies have used these models. However, most studies have only performed kinematic analyses that involve developing a segmented model, defining segmental anatomical reference frames, and calculating segmental and joint angles and angular velocities.

A kinetic analysis requires developing inertial properties for each segment along with the division of GRF and free moment between each segment in the model. Due to these challenges, there have been relatively few kinetic studies using a multi-segmented foot. One study used miniature force sensors (roughly 11-cm^2 area) and footprints on chalk dust to divide the GRF and locate the center of pressure (Scott and Winter, 1993). However, more recent studies have focused on three main approaches for analysis of a two-segmented foot. Among the three, two approaches partition the GRF into the respective segments, whereas the third one does not. The first approach uses a pressure mat and a proportionality assumption theory (MacWilliams et al., 2003; Cowley et al., 2001). The second approach uses two adjacent force platforms and visual targeting (Bruening et al., 2010). The third approach considers kinetics of selective phases of the gait cycle when the GRF acts only on one segment of the foot (Dixon et al., 2012).

MacWilliams et al. (2003) performed the first comprehensive kinetic analysis of the multi-segmented foot model. In dynamic trials, data of the pressure mat and force platforms were combined to separate the GRF to be applied to all six segments of the foot. The pressure data was masked to obtain the normal force and COP for each mask segment throughout the stance phase. Shear forces and free moments from the force plate data were distributed among the six segments in proportion to the percent of normal GRF in each segment at each dynamic frame. The results showed sharp peaks in the power curve at late stance for the talocrural joint indicating power generation. Power absorption peaks were also seen in power curves for medial MTP and hallux MTP joints during late stance. Results obtained by MacWilliams et al. (2003) was similar to their original study (Cowley et al., 2001) that introduced the proportionality assumption theory using the pressure platform. Power profiles obtained by Cowley et al. (2001)

also suggested positive power generation at late stance at the tibiotalar joint and power absorption peak in hallux and medial toes during the same phase of the gait cycle.

Bruening et al. (2010) described a split force platform approach where two adjacent force plates were visually targeted to distribute the GRFs to the adjacent segments. The foot was modeled by three segments: hindfoot, forefoot, and hallux (toes), with the hindfoot and forefoot separated by the mid-tarsal joint and the forefoot and hallux separated by the first MTP joint (Bruening et al., 2012a). For the kinetic analysis, three sub-models of the foot were used (Bruening et al., 2012b). The first sub-model studied the motion, power, and work done between the hindfoot and the rest of the foot separated at the mid-tarsal joint. The second sub-model did the same between the hallux and the rest of the foot separated at the first MTP joint. The third sub-model was the conventional rigid foot model used for comparing the power. These results were combined to give an estimation of work and power using a multi-segmented foot and were compared with the rigid model. Bruening et al. (2012b) also argued that using the proportionality assumption tends to overestimate MTP joint power in late stance.

Dixon et al. (2012) studied kinetics of the Oxford Foot Model. The authors hypothesized that after heel rise, the GRF acts anterior to the tarso-metatarsal joints. Therefore, they adopted a single force platform approach with the assumption that during early stance, the GRF acts posterior to the tarso-metatarsal joints and during late stance, it acts anterior to the joints. The study used the results of the proportionality assumption theory used by MacWilliams et al. (2003) as a comparison. Their results showed that mean power generated at the ankle was greater for the rigid foot model compared to the Oxford Foot Model. However, their model still overestimated ankle power in comparison to the results of MacWilliams et al. (2003). The results also demonstrated non-negligible power generated at the midfoot during late stance. Their main

19

conclusion was that their strategy was better than using a rigid foot model but lacked the accuracy of the proportionality assumption theory. Dixon et al.'s strategy was later tested, comparing their approach and MacWilliams et al.'s approach against the split force platform approach as the gold standard for both the first MTP joint and the mid-tarsal joint (Bruening and Takahashi, 2018). The proportionality assumption theory was indeed found to be more valid than the theory used in Dixon et al. (2012).

Despite differences between the various multi-segment kinetic analyses, all the multi-segment foot studies demonstrated non-negligible power internal to the foot, and reduced ankle power in comparison to a foot modeled as a single rigid segment. An example of power profile is shown in Figure 2 (Bruening et al., 2012b). It is clear from the figure that ankle power is overestimated considerably when using a single rigid body foot (FOOT model) than when using a segmented foot (MID model). Non-negligible power absorption and generation can also be observed in internal foot joints (mid-tarsal and MTP joints).
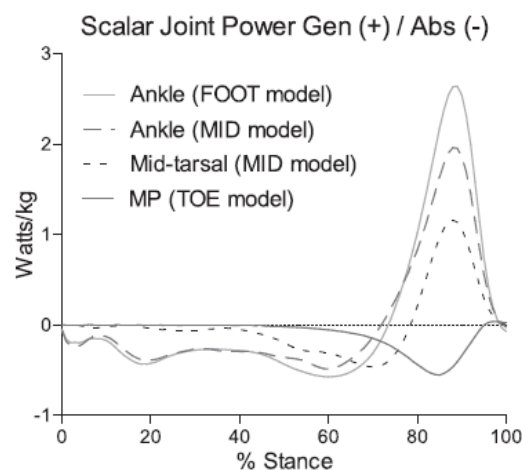
Figure 2 Joint powers calculated using the different sub-models used by Bruening et al., 2012b where solid light lines represent the ankle power obtained using their rigid foot (FOOT) model, longer dashed lines represent ankle power obtained using their multi-segment foot (MID) model,

shorter dashed lines represent mid-tarsal joint power obtained using their MID model, and solid

dark lines represent metatarsophalangeal joint power using their TOE model that had a hallux

segment added to their rigid FOOT model. (Image Source: Figure 5, Bruening et al., 2012b)

2.3   Standing Vertical Jump Studies:

Numerous studies have highlighted the role of lower extremity joint kinetics in vertical jumping.

One of the first inverse dynamic analyses of the standing vertical jump done by Robertson and

Fleming (1987) modeled the foot as a single rigid segment and reported hip and ankle joints as

the major contributors in terms of work done for vertical jump (40% and 35%, respectively).

Their results highlighted the role of the hip, knee, and ankle joints towards the propulsive phase

of the jump. Aragón-Vargas and Gross (1997) compiled a study of different kinesiological

factors such as takeoff velocity, starting position, joint angles at takeoff and joint kinetics before

takeoff that affect performance of vertical jumping. Results of 2D inverse dynamics done in their

study demonstrated that all lower-limb joints (hip, knees, and ankles) generate substantial power

closer to takeoff. Hip power generation peaked prior to knee power peak, immediately followed

by ankle power peak. The peak ankle power magnitude was the highest. The power generation

phase was preceded by a short period of power absorption at all the mentioned joints. Nagano et

al. (1998) modeled the body segments as a four point-mass system by reducing the motion to

pure translation of the mass centers of the segments and only considered vertical joint push-off

force and vertical joint power. Their results showed substantial power generation in the lower

extremity joints preceded by a short period of power absorption. Vanrenterghem et al. (2004)

studied movement strategies to maximize jump performance. The results showed that hip joint

flexion increased with jump height, however, ankle and knee joint flexion did not.

2.4   MTP Joint Contribution in Jumping:

A running vertical jump study modeled the foot as two segments: rear-foot and forefoot, separated at the metatarsophalangeal joints (Stefanyshyn and Nigg, 1998). Using a pressure insole to divide the GRF between the two segments, forces and moments at the first MTP joint were calculated. Average MTP power for all the subjects showed a net power absorption at the first MTP joint of around 500 W at late stance, with a mean energy absorption of 24.5 J. The power absorption phase was preceded by a smaller power generation phase through mid-to-late stance. Another study by Bezodis et al. (2012) compared three different foot models in sprinting. One model divided the foot into fore-foot and rear-foot at the first MTP joint which was similar to the one used by Stefanyshyn and Nigg (1998). The second model was a commonly used single-segment foot with hallux as the distal end. The third model was also a single-segment foot with first MTP joint as the distal end (basically a single-segment rear-foot). Inverse dynamics analysis results suggested that the two single-segment foot models overestimated peak positive ankle and knee joint powers noticeably. Hip power was not significantly overestimated. In contrast, the two-segment foot model showed lesser peak positive ankle and knee powers as well as a phase of power absorption at the first MTP joint at around 75% stance followed by smaller phase of power generation.

2.5   Summary of Approaches:

In multi-segment foot models, most of the power internal to the foot can be attributed to the power at joints internal to the foot. Although the most convincing way to estimate the foot and ankle power may be through using multi-segmented foot models, these models are much more difficult to implement than simply modeling the foot as a single rigid body. Distal foot power and power balance techniques also estimate power internal to the foot as a measure of deviation

from rigid body mechanics and are relatively straightforward to calculate while using a single rigid foot model. Several independent gait studies have been performed using each one of these three power estimation methods separately. However, no previous study has been performed to compare these three approaches for estimating internal foot power. Also, none of these three approaches have been applied to analysis of a standing jump. Hence, the aim of this study was to estimate the foot and ankle power using the two methods for estimating internal foot power with a single rigid foot and the split-force platform approach for a two-segment foot divided at the MTP joints. In doing so, the relative importance of MTP joint kinetics in the takeoff phase of standing vertical jumps was also documented.

3   Procedure:

3.1   Overview:

The method of using two adjacent split-force platforms (Bruening et al., 2010) was used to apportion the GRF and free moment to different foot segments. For distal foot power and power balance calculations, the two split-force platform data were combined as if a single rigid body foot were acting upon a single force platform.

3.2   Description of Model:

3.2.1   Marker Set:

A unilateral, right-side lower limb model with segments and joints distal to the right knee was developed. Markers were placed at anatomical locations to allow for the determination of joint centers and the creation of anatomical reference frames for each segment. The marker set and anatomical reference frames were slightly modified from those described by Bruening et al. (2012a). The most distal segment of their model consisted of only the hallux whereas the model used considered the presence of all the distal phalanges moving together. Markers were placed on bony landmarks as much as possible to reduce soft tissue artifacts. The full marker set with marker description is described in Table 1.

3.2.2   Model Segments:

The study model contains a shank and a two-segment foot. The distal segment is the forefoot containing all five phalanges distal to the MTP joints. The segment of the foot proximal to the MTP joints is the rear-foot. The model hence allows for the analysis of the MTP joint kinematics and kinetics. For the calculation of inertial properties, the rear-foot is further divided into two sub-segments (mid-foot and hind-foot). The mid-foot segment is proximal to the MTP joints and distal to the mid-tarsal joint (MTC). The hind-foot segment is proximal to the MTC joints. All

joints were modeled as 6DOF joints. A detailed description of the joint locations is given in Table 2 and joints at the proximal and distal ends of the segments are shown in Table 3. In addition, a single rigid body foot model was used for the distal foot power and power balance techniques.

Table 1: Marker Set & Locations

Marker Name	Location
Right Foot	
Forefoot	
HLX	Hallux (Centroid of Hallux Nail)
MT1	Head of 1st Metatarsal
MT2	Midway between Head of 2nd and 3rd Metatarsal
MT5	Head of 5th Metatarsal
Rear-foot	
Mid-foot	
NAV	Medial Prominence of Navicular Bone
CUB	Lateral Centroid of Cuboid
Hind-foot	
MCL	Medial Calcaneus (Sustentaculum tali)
LCL	Lateral Calcaneus (Peroneal tubercle)
CAL	Calcaneus (Heel)
LML	Lateral Malleolus
MML	Medial Malleolus
Right Shank	
LKNE	Lateral Femoral Epicondyle
MKNE	Medial Femoral Epicondyle
FBH	Fibular Head
TUB	Tibial Tuberosity
SHN	Anterior Crest of Tibia

Table 2: Location of Joint Centers

Joints	Location
Right Knee (KJC)	Midpoint between LKNE and MKNE
Right Ankle (AJC)	Midpoint between LML and MML
Right Mid-tarsal joint (MTC)	Midpoint between CUB and NAV
Right Metatarsophalangeal joint	Projection half-height from the mid-point of right 2nd and 3rd head of the metatarsals

Table 3: Joints at Segment Endpoints

Segment			Proximal Endpoint	Distal Endpoint
Shank			KJC	AJC
Foot	Rear-foot	Hind-foot	AJC	MTC
		Mid-foot	MTC	MTP
	Fore-foot		MTP	HLX

3.2.3 Inertial Properties:

Mass fractions for shank and foot segment were consistent with anthropometric descriptions

summarized by Winter (2009). Mass fractions for the foot sub-segments were determined via

volumes of associated solids and assuming constant density (Ackland et al., 1988). For inertial

frames, the rear-foot was modeled with two sub-segments based on definitions by Bruening et al.

(2012b) and the foot was modeled with three sub-segments based on definitions of hind-foot and

mid-foot according to Bruening et al. (2012b), and the fore-foot definition developed for this

study. Modeling of the different segments of the foot is shown in Figure 3. The hind-foot was

considered to be a cylinder with its diameter given by the LCL to MCL markers and long axis

given by the MTC to CAL markers. The mid-foot was considered to be an elliptical cylinder

with the major axis given by the NAV to CUB markers and the minor axis length given by the

distance of the MT2 marker from the ground in the vertical direction. The long axis was given by

the MTC to MTP joints. The forefoot was considered to be an elliptical cylinder with major axis

given by the MT1 to MT5 markers, and the minor axis length was given by the distance of the

HLX marker from the ground in the vertical direction. The long axis was defined by the MT1 to

HLX markers. Using the associated volumes, mass centers of the segments were determined.

Then mass and inertial properties of mid-foot and hind-foot were combined to obtain inertial

properties of the rear-foot using the transfer rule for inertia. An instance of the rule for

expressing inertia tensor of hind-foot with respect to the rear-foot COM is shown in Eqn. 3.

$$I^{hf/rfG} = I^{hf/hfG} + I^{hfG/rfG} \qquad \text{Eqn. 3}$$

where, $I^{hf/hfG}$ and $I^{hf/rfG}$ are inertia tensors of the hind-foot with respect to its own COM and

rear-foot COM respectively, and components of $I^{hfG/rfG}$ are given by Eqn. 4.

$$I_{j,k}^{hfG/rfG} = m_{hf}(\|r\|^2\delta_{jk} - r_jr_k) \qquad \text{Eqn. 4}$$

where, m_{hf} is hind-foot mass, r is the position vector from COM of hind-foot to COM of rear-foot, r_j is

the jth element of the position vector r, delta function, $\delta_{jk} = 1$ (if $j = k$), otherwise 0.

A similar process was applied to obtain inertia for the foot combining fore-foot, mid-foot, and

hind-foot. Accordingly, principal axes and principal moments of inertia were calculated using

formulas in Table 4. Inertial properties of the shank were not needed since knee joint kinetics

was not the focus of the study.
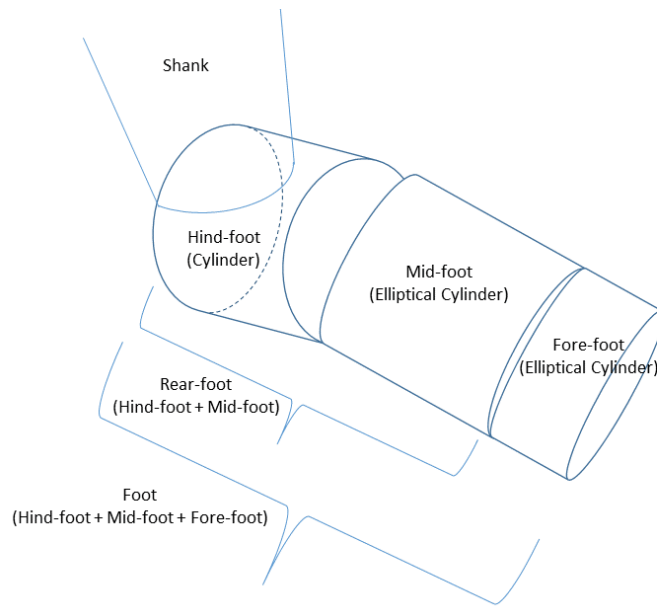
Figure 3 Modeling different segments of the foot

Table 4: Inertial Properties of Segments

Segment	Associated Solids	Segment Volume	Segment Mass
Hind-foot	Cylinder	$V_{hf} = \pi r_{hf}{}^2 (l_{hf})$	$m_{hf} = \dfrac{V_{hf}}{V_{hf} + V_{mf} + V_{ff}}(m_f)$
	$I_{zz} = \dfrac{(m_{hf})r_{hf}{}^2}{2}$ $I_{xx} = I_{yy} = \dfrac{(m_{hf})r_{hf}{}^2}{4} + \dfrac{(m_{hf})(l_{hf})^2}{12}$ Where, $r_{hf} = hind-foot\ diameter\ (LCL\ to\ MCL),$ $l_{hf} = hind-foot\ length\ (CAL\ to\ MTC)$		
Mid-foot	Elliptical Cylinder	$V_{mf} = \pi(a)(b)(l_{mf})$	$m_{mf} = \dfrac{V_{mf}}{V_{hf} + V_{mf} + V_{ff}}(m_f)$
	$I_{zz} = \dfrac{(m_{mf})}{4}(a^2 + b^2)$ $I_{xx} = \dfrac{(m_{mf})a^2}{4} + \dfrac{(m_{mf})(l_{mf})^2}{12}$ $I_{yy} = \dfrac{(m_{mf})b^2}{4} + \dfrac{(m_{mf})(l_{mf})^2}{12}$ Where, $a = major\ axis\ radius\ (half\ distance\ from\ NAV\ to\ CUB),$ $b = minor\ axis\ radius\ (half\ height\ of\ MT2)$ $l_{mf} = mid-foot\ length\ (MTC\ to\ MTP)$		
Fore-foot	Elliptical Cylinder	$V_{ff} = \pi(a)(b)(l_{ff})$	$m_{ff} = \dfrac{V_{ff}}{V_{hf} + V_{mf} + V_{ff}}(m_f)$
	I_{xx}, I_{yy}, I_{zz} are same as mid-foot, $a = (half\ distance\ from\ MT1\ to\ MT5), b = half\ height\ of\ HLX,$ $l_{ff} = fore-foot\ length\ (MT1\ to\ HLX$		

3.3 Experimental Design:

3.3.1 Participant Selection:

Six adult participants (three males and three females) were recruited to volunteer for the study. The participant demographics are shown in Table 5. The participants were individuals who took part in physical activity at least once a week with no persisting effects from an injury or disease to the back, neck, ankles, knees, hips, shoulders, or elbows. Participants were excluded if a medical professional had placed limitations on their current physical activity. All participants

completed a written survey with questions about their age, height, and weight; frequency, duration, and level of physical activity; and past injury history. All participants provided informed consent after reading and signing a consent form that described the study and any potential risks. The protocol was approved by the IRB of Grand Valley State University (Study no. 19-143-H Expiration: December 16, 2020).

Table 5: Demographics of participants in the study

Participant	Age (years, months)	Height (m)	Weight (kg)
1	20y	1.78	68.28
2	26y 11m	1.71	68.48
3	25y 10m	1.73	66.89
4	26y 4m	1.72	63.94
5	20y 6m	1.63	63.68
6	24y 6m	1.66	60.25
Average			
Male Participants	24.3 ± 3.7 y	1.74 ± 0.04	67.9 ± 0.9
Female Participants	23.8 ± 3.0 y	1.67 ± 0.04	62.6 ± 2.1
Overall	24.0 ± 3.0 y	1.7 ± 0.05	65.3 ± 3.2

3.3.2   Equipment Setup:

Jumping trials were captured using a Vicon motion capture system (Vicon Motion Systems Ltd., Los Angeles, CA) consisting of 16 cameras and two AMTI force plates (Advanced Mechanical Technology Inc., Watertown, MA). The motion capture system was calibrated, and force plates were zeroed before each data collection session. A set of reflective markers was used to collect the data. The 3D locations of the reflective markers were captured by the 16 cameras operating at 120 Hz. The force plates captured ground reaction forces, free moments, and locations of centers

of pressure at 1200 Hz. Vicon Nexus software (Version 2.81) was used to process the raw data and export it for further data analysis.

3.3.3   Data Collection:

After each participant granted informed consent for the protocol, the height of each participant was measured. Each participant was instructed to perform the trials barefoot. Sixteen reflective markers were placed on the skin of key landmarks of the participant's right leg and foot with double-sided tape. Marker placement was verified by a skilled professional physical therapist with an experience of more than 25 years. The marker positions were documented with still photography. The participants then were asked to warm up by jogging on a treadmill at a self-selected, comfortable speed for about 5 minutes. They were then allowed to stretch if desired. The participants were asked to perform several practice jumps (advancing from submaximal to maximal effort standing vertical jumps) three to four times prior to data acquisition. Following warm up, one second of marker position data was collected with the participant standing with both feet on one force platform. The marker positions and initial starting position are shown in Figure 4. The purpose of this was to determine participant weight, segmental center of mass locations, and joint center locations.

The participants were then asked to perform maximum effort vertical jumping trials. For the starting position, they were directed to align the distal edge of MT2 marker of the right foot above the line connecting two adjacent force plates, as depicted in Figure 4. They were also instructed to place their left foot completely outside the two force plates where their right foot was placed. Six jumping trials were recorded for each participant. Video of front view and right lateral view of the jumping trials were also recorded for documentation purposes. Marker placement was monitored after every jump and extra tape was added to ensure markers did not

move. The force plate data and marker continuity were checked to confirm that data was properly collected. After confirming that all trials were good, the markers were removed.
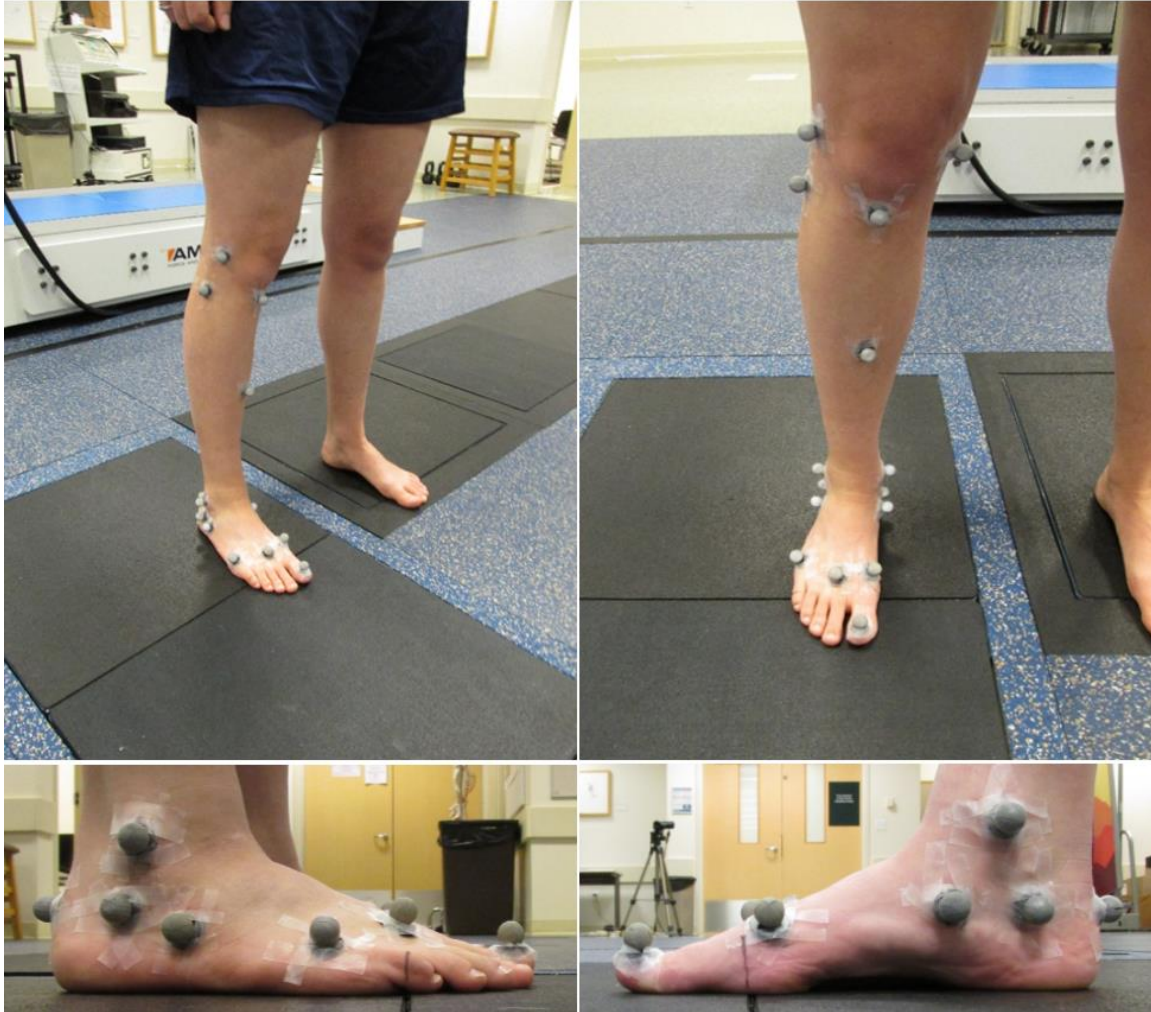

Figure 4: Marker placement and starting position for takeoff (a) perspective view (b) front view (c) lateral view (d) medial view. Note that MT2 marker is placed exactly posterior to the common edge of the two adjacent force plates. A pencil was used to mark a line on the participant's foot to aid with consistency of the starting position.

3.3.4 Data Processing:

3.3.4.1 Initial processing:

The raw data exported out of Vicon Nexus software contained 3D force plate data (forces, moments, locations of COP for each force plate) and 3D coordinates of each marker location throughout each jump. Using custom code in MATLAB, Version 2018a (Mathworks, Natick, MA), the data for all jumps were processed. Residual analysis on all marker and force plate data for all subjects and trials was completed using the method described by Winter (2009) and Yu et al. (1999). The results showed a range of 7.1 to 11.4 Hz, with mean of 10.4 Hz, mode of 10.9 Hz, and median of 10.4 Hz. All data was then filtered at 10.4 Hz using a 4th-order, dual-pass, low-pass Butterworth filter. Since the force plates acquired data at 10 times greater frequency than the motion capture cameras, the force data was also subsampled down by a 1:10 ratio after filtering.

3.3.4.2 Kinematic Analysis:

From the static trial, technical reference frames were developed to calculate joint centers in the global reference frame. Then anatomical reference frames were developed for the shank and foot (and separately for rear-foot, hind-foot, mid-foot, and fore-foot). Hind-foot and mid-foot definitions were used only to define inertial parameters for the rear-foot. Joint centers were expressed in the segmental anatomical reference frames for use in the dynamic trials. Center of mass locations and inertia tensors expressed in the anatomic reference frames were calculated for each segment. 3D segment angles, angular velocities, and angular accelerations were also determined. Force plate data from the static trial were used to calculate the total body weight. Using the segment mass fractions described in Winter (2009), segmental masses for each participant were also determined.

For each jumping trial, the analysis was performed on the last 1.2 seconds before takeoff. This time duration was chosen since it was enough to incorporate the downwards countermovement before takeoff for the vertical jump. Technical reference frames were developed and using joint center locations from static trial, global coordinates of joint centers were determined. Then, anatomical reference frames for the shank, foot, rear-foot, and fore-foot were created. From anatomical reference frames, segment rotation matrices were evaluated. Using Cardan Euler sequence (X-Y'-Z''), euler angles were calculated for each segment followed by segment angular velocities and angular accelerations. Center of mass locations for each segment were calculated for the dynamic frames. Segment mass center velocities and accelerations were also calculated using finite difference formulas.

3.3.4.3 Kinetic Analysis:

Using Multi-Segment Foot:

Inverse dynamics was used to evaluate forces and moments at distal and proximal ends of each segment. The 3D forces and moments for a segment were resolved at two points plus the segment weight as shown in Figure 5. However, for the rear-foot segment, the forces and moments were resolved at three points in the segment plus the rear-foot weight as shown in Figure 6. The three points of application were the ankle joint, MTP joints, and the COP of one of the force plates.
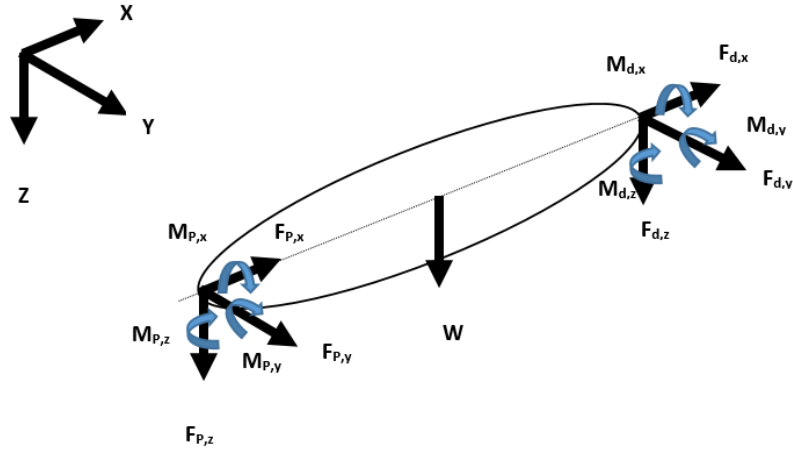
Figure 5 General case for inverse dynamics calculations (where W is segment weight, $\boldsymbol{M}_{p,x}$, $\boldsymbol{M}_{p,y}$, $\boldsymbol{M}_{p,z}$ are proximal joint moments, $\boldsymbol{F}_{p,x}$, $\boldsymbol{F}_{p,y}$, $\boldsymbol{F}_{p,z}$ are proximal joint intersegmental forces, in three orthogonal directions. Likewise, $\boldsymbol{M}_{d,x}$, $\boldsymbol{M}_{d,y}$, $\boldsymbol{M}_{d,z}$, $\boldsymbol{F}_{d,x}$, $\boldsymbol{F}_{d,y}$, $\boldsymbol{F}_{d,z}$ are distal joint moments and intersegmental forces in three orthogonal directions)
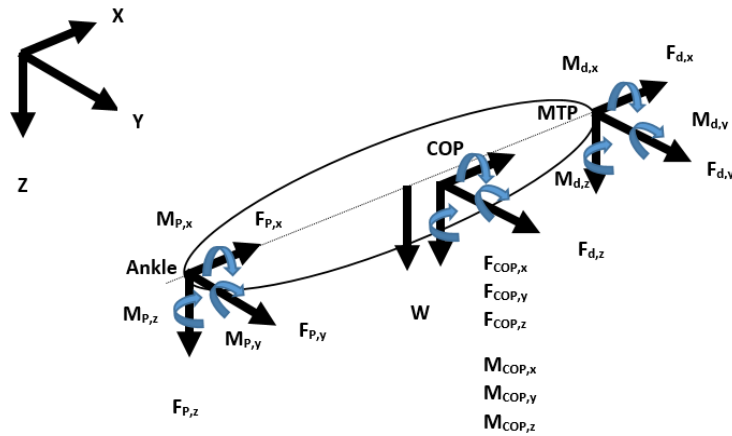
Figure 6 Specific case for inverse dynamics calculations for rear-foot (specific case expanded from Figure 5 where ankle is the proximal joint, MTP joint is the distal joint and there is a second distal end at COP (center of pressure) of the rear-foot. $\boldsymbol{M}_{COP,x}$, $\boldsymbol{M}_{COP,y}$, $\boldsymbol{M}_{COP,z}$ are ground reaction moments and $\boldsymbol{F}_{COP,x}$, $\boldsymbol{F}_{COP,y}$, $\boldsymbol{F}_{COP,z}$ are ground reaction forces in three orthogonal directions.)

After resolving forces and moments, the equations of motion were written as shown in Eqn. 5
and Eqn. 6:

$$\sum \boldsymbol{F} = \begin{bmatrix} \sum F_x \\ \sum F_y \\ \sum F_z \end{bmatrix} = \begin{bmatrix} F_{p,x} + F_{d,x} \\ F_{p,y} + F_{d,y} \\ F_{p,z} + F_{d,z} - W \end{bmatrix} = m \begin{bmatrix} a_x \\ a_y \\ a_z \end{bmatrix} \qquad \text{Eqn. 5}$$

$\boldsymbol{F}$ is the resultant force vector, W is the magnitude of the segment weight, and a_x, a_y, a_z are the
components of acceleration of the segment in the x, y, and z directions, respectively.

$$\sum \boldsymbol{M}_G = \boldsymbol{M}_d + \boldsymbol{r}_d \times \boldsymbol{F}_d + \boldsymbol{M}_p + \boldsymbol{r}_p \times \boldsymbol{F}_p = \boldsymbol{I}_G \boldsymbol{\alpha} + \boldsymbol{\omega} \times \boldsymbol{I}_G \boldsymbol{\omega} \qquad \text{Eqn. 6}$$

$\boldsymbol{M}_G$ is the resultant moment around the segment COM, $\boldsymbol{M}_p$ and $\boldsymbol{M}_d$ are proximal and distal joint
moments, $\boldsymbol{F}_p$ and $\boldsymbol{F}_d$ are proximal and distal joint intersegmental forces, $\boldsymbol{r}_p$ and $\boldsymbol{r}_d$ are position
vectors from segment COM to the proximal and distal joints, $\boldsymbol{I}_G$ is the inertia tensor of the
segment around its COM, and $\boldsymbol{\alpha}$ and $\boldsymbol{\omega}$ are angular acceleration and angular velocity of the
segment.

For the rear-foot segment, Eqn. 5 and Eqn. 6 included the additional $\boldsymbol{F}_{COP}$ and M_{COP} terms
respectively on the left-hand side of the equations.

There were six equations and six unknowns each for two segments with a total of 12 equations
and 12 unknowns. The system was a fully determined system, allowing solving the system for
3D forces and 3D moments at the metatarsophalangeal and ankle joints in a bottom-up inverse
dynamic analysis.

Using Rigid Body Foot:

For distal foot power and power balance calculations, the foot was modeled as a rigid body. The
ground reaction force and free moment data from the two force plates were combined as if the

two force plates were a single force plate. The combined COP, GRF and free moment were considered to be acting upon a single, rigid-body foot, as shown in Figure 7. In the figure, F_1 and F_2 represent GRF vectors, τ_1 and τ_2 represent free moment vectors, and r_1 and r_2 represent COP position vectors of plates 1 and 2, respectively. The resultant force F_c on the combined force plate is given by Eqn. 7 and resultant free moment τ_c and resultant COP position vector r_c can be calculated with Eqn. 8.

$$F_c = F_1 + F_2 \qquad\qquad \text{Eqn. 7}$$

$$r_1 \times F_1 + r_2 \times F_2 + \tau_1 + \tau_2 = r_c \times F_c + \tau_c \qquad\qquad \text{Eqn. 8}$$

From the first equation, F_c was calculated. In the second equation, the remaining unknowns were r_c and τ_c. However, for ground reaction moments, the x and y components of the free moment vector, τ_c, were zero and the z component of COP position vector r_c was also zero. Hence, x and y components of r_c and z component of τ_c were calculated from the three component equations of Eqn. 8.

For the single rigid foot, there were six equations of motion and six unknowns (ankle joint forces and moments). This system too was fully determined. Solving this system in a bottom up inverse dynamics approach gave forces and moments at the ankle joint.
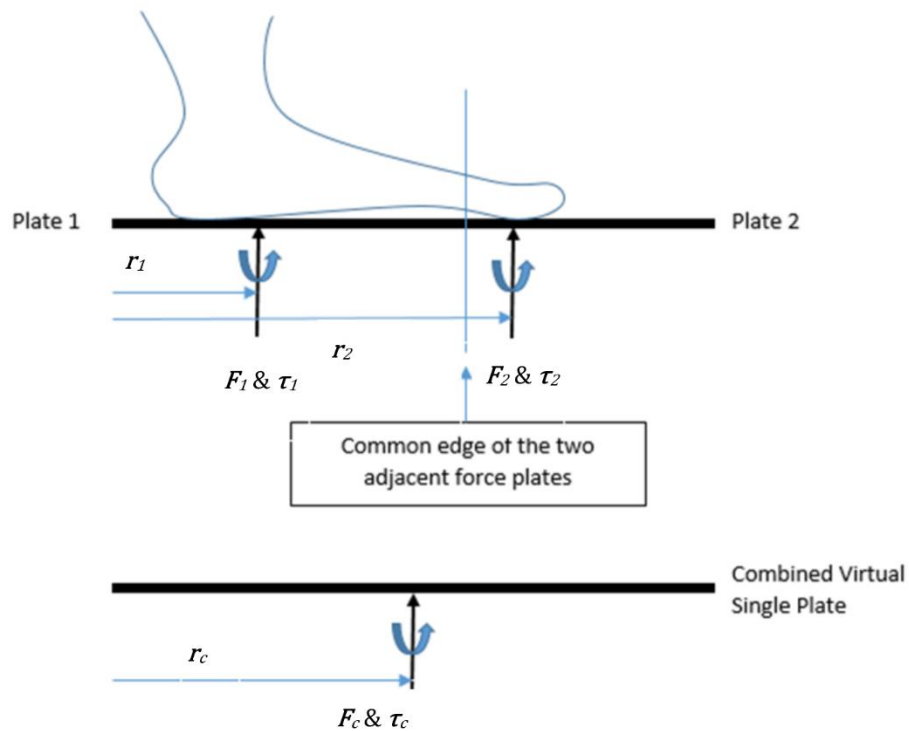
Figure 7 Combining adjacent force plates into one virtual resultant plate (where F_1 and F_2 represent GRF vectors, τ_1 and τ_2 represent free moment vectors, and r_1 and r_2 represent COP position vectors of plates 1 and 2, respectively, and F_c, τ_c, and r_c represent the combined resultant GRF, free moment and COP position vector respectively.)

3.3.4.4 6DOF Power and Work:

Multi-segment Foot:

6DOF power was calculated at MTP and ankle joints using Eqn. 9:

$$P_{joint} = P_{distal} + P_{proximal} \qquad \text{Eqn. 9}$$

P_{distal} and $P_{proximal}$ are power of the segment distal and proximal to the joint, given by the Eqn. 10 and Eqn. 11.

$$P_{distal} = \boldsymbol{M}_{joint,d} \cdot \boldsymbol{\omega}_d + \boldsymbol{F}_{joint,d} \cdot \boldsymbol{v}_d \qquad\qquad \text{Eqn. 10}$$

$$P_{proximal} = \boldsymbol{M}_{joint,p} \cdot \boldsymbol{\omega}_p + \boldsymbol{F}_{joint,p} \cdot \boldsymbol{v}_p \qquad\qquad \text{Eqn. 11}$$

$\boldsymbol{M}_{joint,d}$ and $\boldsymbol{M}_{joint,p}$ are distal and proximal joint moments, $\boldsymbol{\omega}_d$ and $\boldsymbol{\omega}_p$ are segment angular velocities, $\boldsymbol{F}_{joint,d}$ and $\boldsymbol{F}_{joint,p}$ are distal and proximal intersegmental forces, and $\boldsymbol{v}_d$ and $\boldsymbol{v}_p$ are distal and proximal joint velocities calculated by numerical differentiation of the position vector of the distal and proximal joints of the segment in the global reference frame.

The 6DOF power was then integrated over takeoff time to calculate 6DOF work.

Distal Foot Power:

Distal foot power (Siegel et al., 1996) was calculated using Eqn. 1:

$$P_{dfp} = \boldsymbol{F}_{GRF} \cdot \boldsymbol{v}_d + \boldsymbol{M}_{free} \cdot \boldsymbol{\omega}_f$$

$\boldsymbol{F}_{GRF}$ is the ground reaction force acting on the foot at the center of pressure (COP), $\boldsymbol{M}_{free}$ is the free moment acting on the foot, $\boldsymbol{\omega}_f$ is the angular velocity of the foot, and $\boldsymbol{v}_d$ is the distal foot velocity calculated using Eqn. 2.

$$\boldsymbol{v}_d = \boldsymbol{v}_G + \boldsymbol{\omega}_f \times \boldsymbol{r}_d$$

$\boldsymbol{v}_G$ is the velocity of the mass center of the foot, $\boldsymbol{r}_d$ is the position vector from the foot's mass center to the COP.

Power Balance:

Power imbalance for a segment (Winter, 2009) was calculated using Eqn. 12:

$$P_{imbal} = P_{segment} - \frac{dE}{dt} \qquad\qquad \text{Eqn. 12}$$

where $P_{segment}$ is segmental power calculated using Eqn. 13, and $\frac{dE}{dt}$ is rate of change of segmental energy.

$$P_{segment} = \boldsymbol{M}_{joint,d}.\,\boldsymbol{\omega}_s + \boldsymbol{F}_{joint,d}.\,\boldsymbol{v}_d + \boldsymbol{M}_{joint,p}.\,\boldsymbol{\omega}_s + \boldsymbol{F}_{joint,p}.\,\boldsymbol{v}_p \qquad \text{Eqn. 13}$$

$\boldsymbol{M}_{joint,d}$ and $\boldsymbol{M}_{joint,p}$ are moments at the distal and proximal joints for the segment, $\boldsymbol{F}_{joint,d}$ and $\boldsymbol{F}_{joint,p}$ are joint intersegmental forces at the distal and proximal ends, $\boldsymbol{\omega}_s$ is the segment angular velocity, and $\boldsymbol{v}_d$ and $\boldsymbol{v}_p$ are the distal and proximal joint velocities.

For the time rate of segmental energy change, $\frac{dE}{dt}$, the total energy of the segment was numerically differentiated using finite differencing. The total energy of the segment was the sum of kinetic and potential energies determined using the following formulas:

$$\text{Kinetic Energy, } T \ = \ \tfrac{1}{2}\, m_s \boldsymbol{v}_G.\,\boldsymbol{v}_G \ + \ \tfrac{1}{2}\, \boldsymbol{\omega}_s.\,\boldsymbol{I}^{s/G}\boldsymbol{\omega}_s \qquad \text{Eqn. 14}$$

$$\text{Potential Energy, } V \ = \ m_s g\, r_z^G \qquad \text{Eqn. 15}$$

$$\text{Total Energy, } E \ = \ T \ + \ V \qquad \text{Eqn. 16}$$

m_s, $\boldsymbol{v}_G$, $\boldsymbol{\omega}_s$ is, respectively, the mass, mass center velocity, and angular velocity of the segment, $\boldsymbol{I}^{s/G}$ is the inertia tensor for the segment with respect to its mass center, and r_z^G is the z-axis component of the position vector to the mass center.

6DOF power was also calculated for the ankle joint with the single rigid body foot.

3.3.4.5 Normalization:

All results (power as well as work) were normalized by mass times shank length for each subject. Similar to the technique used in Zelik et al. (2015), the normalized values were re-dimensionalized again by multiplying the results using average mass times average shank length. This way of normalization preserved the original units for power (W) and energy (J).

3.3.4.6 Comparison of Methods:

Statistical analysis for the results after normalization and non-normalization was generated using SAS software, Version 9.4 of the SAS System for Windows (SAS Institute Inc., Cary, NC, USA). To determine whether there was a difference in three methods (MTP power, distal foot power, and foot power imbalance) used to calculate foot power and work, one-way within repeated measures ANOVA was implemented (value of alpha used was 0.05) and Bonferroni adjustments were applied. These analyses were conducted using the PROC MIXED function in SAS. Descriptive statistics including the mean power and work of the foot and corresponding confidence intervals were obtained using PROC MEANS. The same process for statistical analysis was repeated for ankle power and ankle work obtained from the two different approaches (rigid foot and multi-segment foot).

4 Results:

4.1 Foot Power and Work:

Distal foot power, foot power imbalance and MTP joint power for 1.2 seconds before takeoff are displayed along with 95% confidence intervals in Figure 8 . Significant differences can be seen between all three methods. The three plots start diverging at 0.3 seconds before takeoff and are clearly different at around 0.1 second before takeoff. However, the plots converge closer to takeoff, i.e. time 0. Distal foot power shows peak power absorption of 111 W in the foot followed by a peak power generation of 102 W. Foot power imbalance plot had three main landmarks: a minimal peak power generation of 6 W around 0.15 to 0.1 seconds before takeoff, a 31 W peak power absorption around 0.1 to 0.05 seconds before takeoff, and a 135 W peak power generation even closer to takeoff. In the MTP joints, power absorption was minimal (~ 7 W at around 0.3 seconds before takeoff). However, a peak power generation of 127 W was observed close to takeoff.

The least square mean estimate for distal foot work was -4.0 ± 1.0 J whereas work from foot power balance and MTP work were positive at 1.8 ± 1.1 J and 5.1 ± 0.5 J, respectively (Figure 9). Table 6 shows that the least squares mean estimate for the difference between distal foot work and MTP joint work (9.1 J) was higher than the other two pairwise comparisons (5.7 J between distal foot work and work from foot power balance, and 3.3 J between MTP joint work and work from foot power balance).
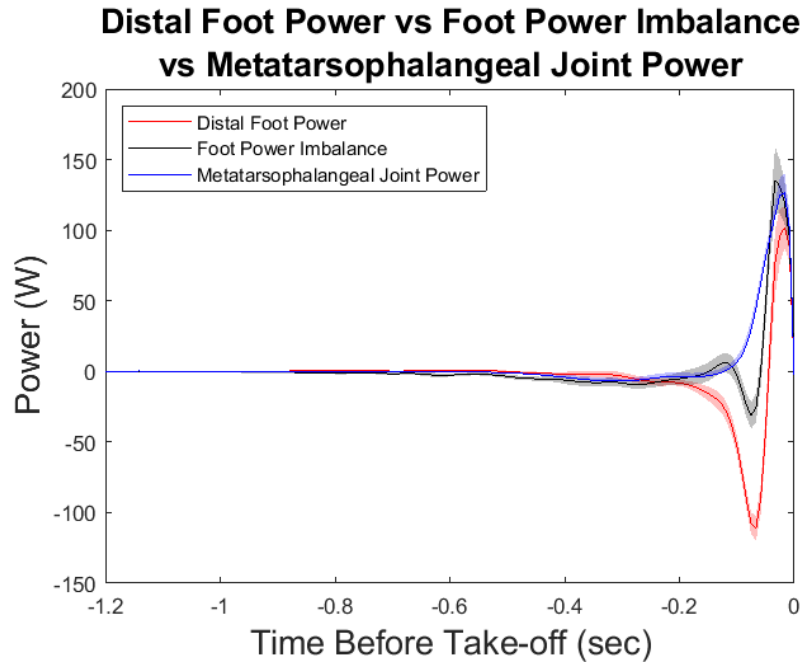
Figure 8 Comparison of mean values for distal foot power versus foot power imbalance versus
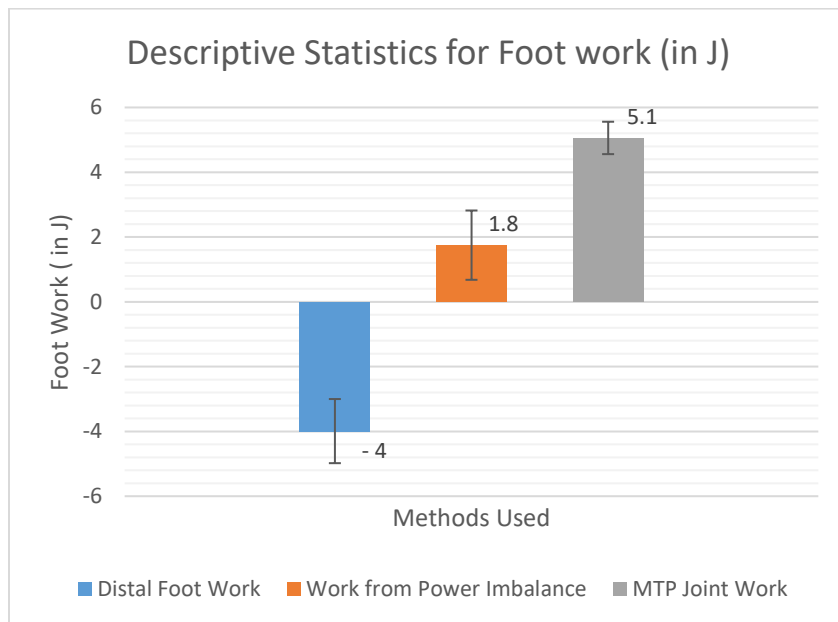
MTP joint power (with 95% confidence interval bands)

Figure 9 Descriptive statistics of footwork (numbers represent mean values and bars represent

95% confidence intervals)

Table 6: Differences between methods for calculating footwork

Comparison	Difference ± 95% CI	p-value
FPI – DFP	5.7 ± 1.2 J	**<0.0001**
MTP – DFP	9.1 ± 1.2 J	**<0.0001**
MTP – FPI	3.3 ± 1.2 J	**<0.0001**

4.2 Ankle Power and Work:

Ankle power obtained using rigid foot model and multi-segment foot model are compared in Figure 10 along with 95% confidence intervals. No differences can be seen in ankle power obtained using the two methods, except at around 0.1 seconds before takeoff where peak ankle power calculated using rigid foot is slightly lower than the peak power using multi-segment foot. The general trend of the plots showed that power is absorbed at the ankle at around 0.4 to 0.3 seconds before takeoff, with a peak power absorption of 43 W. After the power absorption phase, the ankle generated large power (696 W with single rigid foot and 705 W with multi-segment foot) from 0.25 seconds before takeoff to takeoff, peaking at 0.05 seconds before takeoff. The confidence intervals for both curves almost completely overlap, with only a slight difference seen during peak power generation.

The ankle work values calculated using the rigid foot model and multi-segment foot model (Figure 11) were very similar (58.3 ± 3.1 J and 59.9 ± 3.4 J respectively) with a statistically significant difference of only 1.5 J (p = 0.0004).
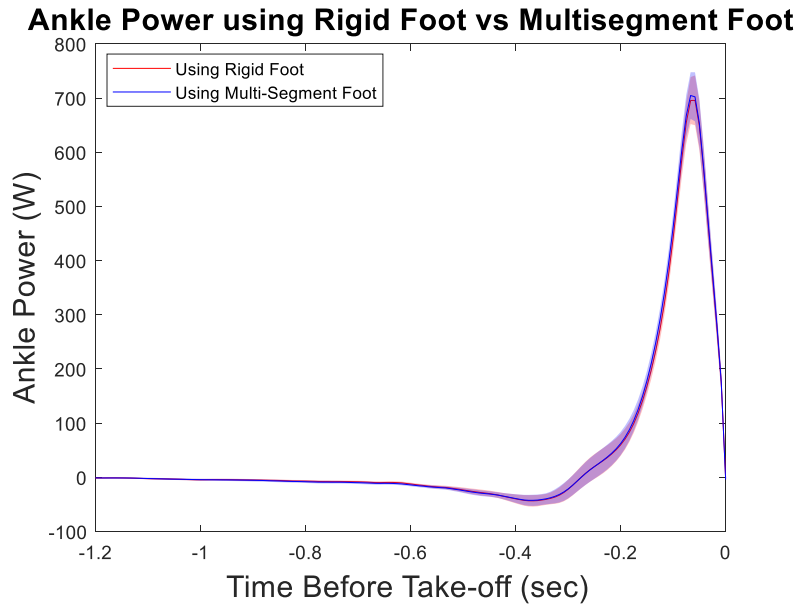
Figure 10 Comparison of mean values for ankle power using rigid foot model versus multi-segment foot model (with 95% confidence interval bands)
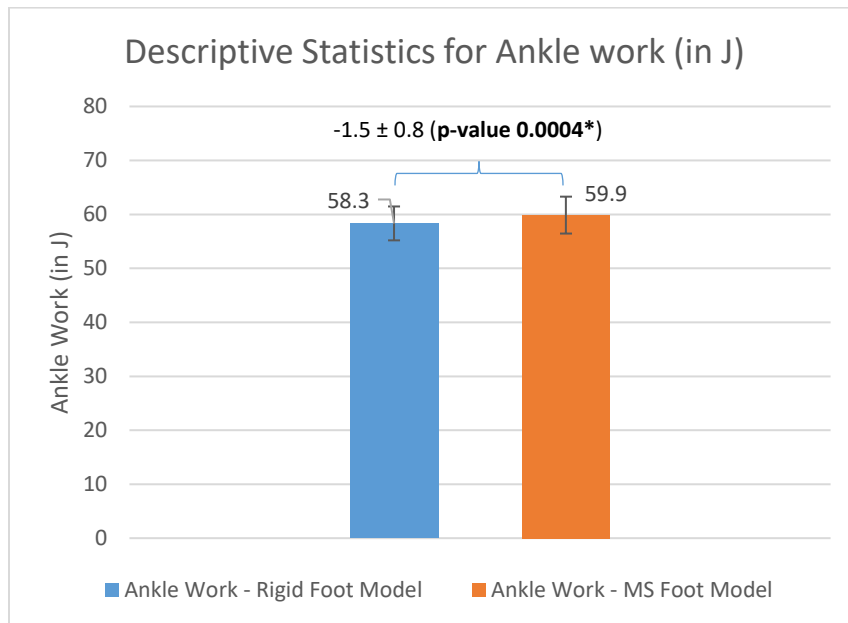

Figure 11 Descriptive statistics for ankle work and differences between methods for calculating ankle work (numbers represent mean values and bars represent 95% confidence intervals)

The similarities between ankle power obtained using the two different foot models motivated a further exploration of the markers used for defining the anatomical reference frame of the rear-foot. The markers used for defining the anatomical reference frame of the rigid foot model were on the calcaneus, and first and fifth metatarsal heads, which were all essentially on the rear-foot. Since the two-segment foot model developed for this study considered rear-foot as a rigid segment, a different set of three markers (on the calcaneus, navicular, and cuboid) were considered fors representing the anatomical reference frame of the rear-foot. After these modifications, a new set of ankle power results were calculated (Figure 12). The graphs show that peak ankle power obtained using the two methods is clearly different and that the rigid foot model may overestimate the ankle power when compared to the multi-segment foot using the changed marker set. Similarly ankle work obtained using the modified multi-segment foot model also changed to 52.49 ± 3.41 J as shown in Figure 13, with a statistically significant difference of 5.84 ± 1.04 J. The ankle work obtained using rigid body fool were not affected by the change.
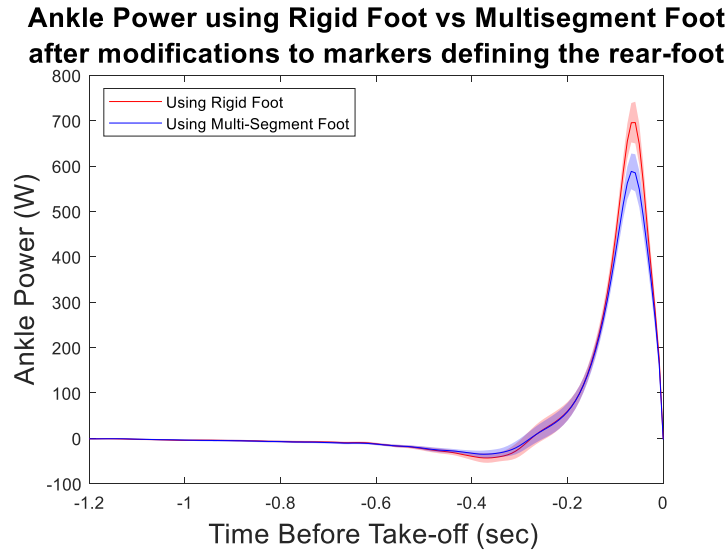
Figure 12 Ankle power using rigid foot vs multi-segment foot (with 95% Confidence Interval

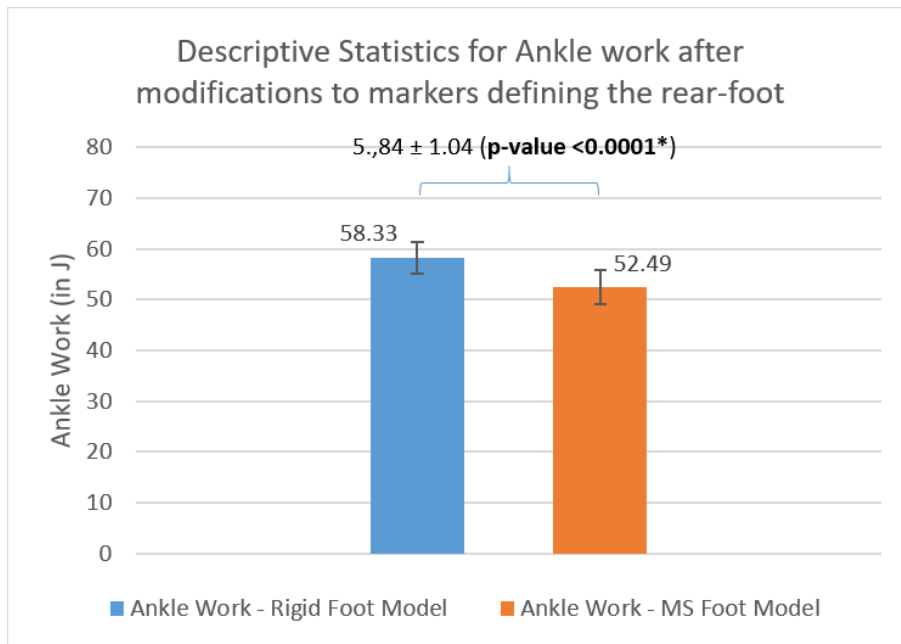bars) using CAL, NAV, and CUB markers for defining the rear-foot's anatomical reference

frame.

Figure 13 Descriptive statistics of ankle work after the modifications to the markers defining the

rear-foot (numbers represent mean values and bars represent 95% confidence intervals)

5   Discussion:

With the underlying assumption of a rigid body model, studying the foot mechanics is relatively simple but essentially flawed. This is because the foot is not a rigid body, owing to the various joints as well as soft tissue deformations internal to the foot. Numerous studies have investigated non-rigid foot mechanics by looking at the power generated or absorbed by the foot. However, no study previously compared different approaches for modeling the non-rigid foot. Hence, the primary aims of the study were to compare three such methods to calculate the power internal to the foot and two methods to calculate ankle power in standing vertical jumps. For the foot, the methods were distal foot power, power balance technique, and studying kinetics of the MTP joints. For the ankle, the methods were using a rigid foot versus a multi-segment foot model.

5.1   Foot Power and Foot Work:

The general trend of the foot power graph from Figure 8 indicated that MTP power and distal foot power were significantly different from each other. It can also be seen that foot power imbalance had a dip around 0.11 to 0.06 seconds before takeoff, around the same time that distal foot power dipped too. Otherwise, before 0.15 seconds and after 0.05 seconds before takeoff, foot power imbalance and MTP power were closer to each other. Due to these differences in the powers, foot work values calculated by integrating the powers were significantly different as well, as depicted in Figure 9. Since the MTP joints mostly generated power, the work done at the MTP joints was also positive with a mean estimate of 5.1 J. Since distal foot power plots showed the greatest power absorption peak, distal foot work was negative at – 4 J. Pairwise comparisons between the three methods showed that the minimum difference was in between work from power balance and MTP work at 3.3 J. This was also reflected in the power plots as mentioned previously. It was clearly observed in the foot power graphs that there was power absorption in

47

the foot. However, there was no substantial power absorption at the MTP joints. The power absorption can hence be attributed to the internal structures of the foot either distal or proximal to the MTP joints. Other joints in the foot such as mid-tarsal center as discussed in Bruening et al. (2012b) and tarsometatarsal joints as discussed in MacWilliams et al. (2003) as well as other soft-tissue interactions could have contributed to the power absorption terms.

Distal foot power has not been previously studied in jumping. Gait studies of distal foot power (Siegel et al., 1996 and Zelik et al., 2018) have shown that right before toe-off, there is increased peak power absorption in the foot. Siegel et al. (1996) attributed it to the anterior and superior movement of the foot in preparation of propelling the foot for swing phase. Zelik et al. (2018) showed that not incorporating the distal foot power term would overestimate ankle power right before toe-off phase of gait. Distal foot power for standing vertical jump from our study indicated a peak power absorption of 102 W around 0.1 seconds before takeoff. However right before takeoff, there was peak power generation of 111 W. Since power is absorbed in the foot, comparison of 6DOF ankle power including and excluding the distal foot power term showed that including the distal foot power decreased the peak ankle plus foot power generated by 100 W. The results were analogous to the ones by Zelik et al. (2018) as shown in Figure 14. Siegel et al. (1996) also suggested that there was a change in sign of distal foot velocity right at toe-off. However, the effect on distal foot power in gait due to the positive distal foot velocity was not substantial. As seen for standing vertical jumps, the effect was substantial causing power generation in the foot right at takeoff. This significant difference in these patterns can be attributed to the greater propulsive power needed in vertical jumping than in push-off for gait.
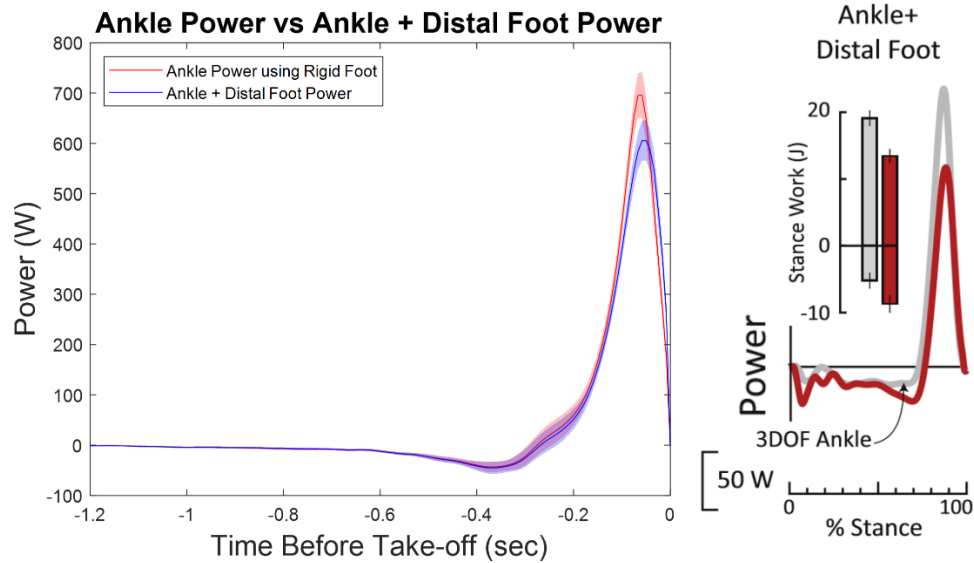
Figure 14 Comparison of the effects of distal foot power on ankle power in the standing vertical jump (left, our study) versus walking (Figure on the right is a portion excerpted from Figure 3, Zelik et al., 2018. The gray line represents 3DOF ankle power and red line represents sum of 6 DOF ankle power and distal foot power).

The results for foot power imbalance shown in Figure 8 also indicated a pattern similar to distal foot power. The power absorption peak of distal foot power was smaller (31 W compared to 111 W), and the power generation peak was higher (135 W compared to 102 W). Preceding the dip in power, there was a small positive power imbalance at 0.125 seconds before takeoff. The components of foot power imbalance (i.e., segmental power flow and energy change rate) for this study too followed the pattern observed in gait studies by Robertson and Winter (1980), as shown in Figure 15. The results of their walking study showed that at terminal stance, segmental energy change rate for the foot increased, whereas a peak power flow of 100 W into the foot was followed by power flow out of the foot of around 50 W. The results of this standing vertical jump study showed a similar pattern, peak power of 40 W flowing into the foot followed by power flow of 98 W out of the foot, whereas segmental energy change rate increased towards

takeoff. The greater power flow out of the foot in vertical jumping versus walking implies the

foot generated greater power for propelling the body vertically upward for the jump.
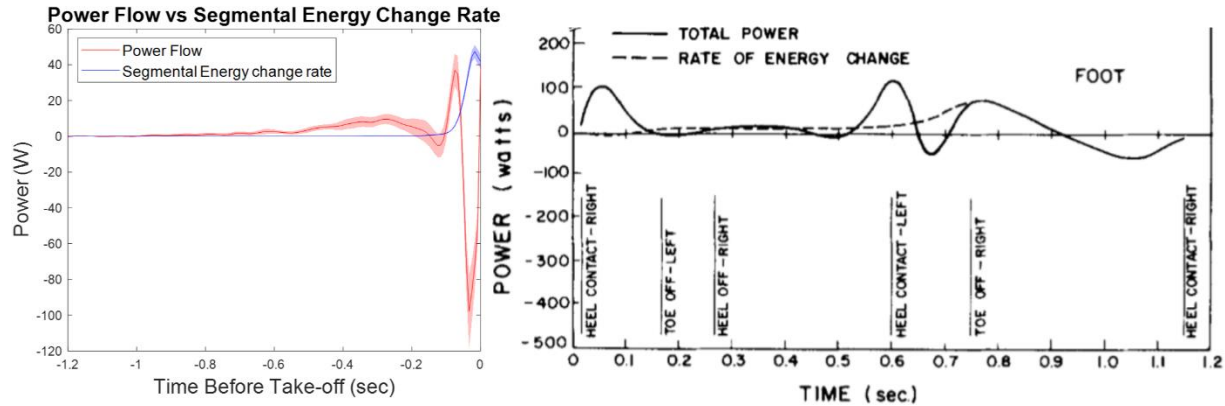

Figure 15 Comparison of difference between segmental power flow & energy change rate of the

foot in standing vertical jump (left, our study) vs walking (Figure on the right is a portion

excerpted from Figure 7, Robertson and Winter, 1980. The dashed line represents segmental

energy change rate whereas solid line represents power flow in/out of the segment).

The differences seen between distal foot power and foot power imbalance motivated further

exploration of the significance of these power terms. Foot power imbalance was simply

calculated as the difference between power flow in/out of the foot and the segmental energy

change rate. Therefore, it simply was an indicator of how much power was lost/gained inside the

foot. Regardless of the foot being considered as rigid or non-rigid, the technique to calculate foot

power imbalance is a mathematically consistent method for documenting internal foot power. On

the other hand, the theoretical foundation and the proper application of the distal foot power

technique introduced by Siegel et al. (1996) is not quite clear. One of the major motivations for

using distal foot power is the understanding that the foot is not rigid, yet the equation for

calculating the distal foot velocity is a rigid body kinematics equation. One way of interpreting

the distal foot power formulation is that it estimates the power due to deviations from the rigid

body state of the foot. However, by definition, the formula for distal foot power only considered power contributions due to the non-rigid motion of the COP with respect to the foot COM. The method does not include power contributions from other portions of the foot. On the other hand, foot power imbalance, as mentioned previously, includes power contributions from all internal sources and hence may be a more complete estimation for power due to the non-rigid nature of the foot. The current study is the first to systemically compare the two methods and the results call for further exploration of the methods for jumping and other movements when the energetics of the distal lower extremities are of interest. These explorations could provide an insight into the possible interchangeable use of the two methods.

A portion of foot power can be attributed to the metatarsophalangeal joints. Results for MTP joint power suggested that the joints are important sources of power generation for standing vertical jumps. Contrasting to these results, kinetic analysis of the joints in walking have shown major power absorption after 75% stance (Bruening et al., 2012b, and MacWilliams et al., 2003). Running vertical jump and long jump studies done by Stefanyshyn et al. (1998) also showed power absorption in the first MTP joint right before takeoff (higher for running long jump). A sprinting study done by Bezodis et al. (2012), however, showed that power was generated in the first MTP joint at late stance (after ~ 90% stance). This phase was preceded by a higher power absorption phase (50% stance to 90% stance). The power absorption seen at the MTP joints in walking, running, or running vertical or long jump may be attributed to the braking that occurs while planting the foot and bringing the swing foot forward. This braking period was not seen in the standing vertical jump as the jumper started from rest and performed a vertical countermovement jump. During downward countermovement, the jumpers squatted a bit which may have stored some stretch-induced energy. However, this dissipation was not as large as the

power dissipated in running vertical jump as observed by Stefanyshyn and Nigg (1998). This may explain why only large power generation and very small absorption was observed at the MTP joints in standing vertical jumps of this study. All these different studies have shown that the contributions of the MTP joints depend upon the type of activity being performed. It is, however, clear that the MTP joints make meaningful positive contributions to the increasing performance in jumping.

5.2 Ankle Power and Ankle Work:

Previous studies that have looked at ankle power in standing vertical jump using rigid foot models have obtained similar results. The results of ankle power in the sagittal plane studied by Aragón-Vargas and Gross (1997) showed high resemblance to the pattern shown in Figure 10. Both graphs showed a slight power absorption at around 0.35 seconds before takeoff, followed by steady power generation at around 0.2 seconds before takeoff, which was immediately followed by a rapid increase in power generated at the ankle at around 0.05 seconds before takeoff. Similar ankle power profiles were also observed in the results reported by Vanezis et al. (2005).

The ankle power profiles obtained using the rigid foot model and the multi-segment foot model were very similar to each other (Figure 10). Ankle power using multi-segment foot model was only slightly higher than the power obtained using rigid foot model. This slight difference was supported by the ankle work estimates from descriptive statistics in Figure 11. The close similarity of the ankle power curves using the two methods was likely due to definition of the rigid foot model and the rear-foot segment of the multi-segment foot. Both the rear-foot and rigid foot used the head of first and fifth metatarsals and calcaneus markers to define the anatomical reference frames. Hence, the kinematics and kinetics of rear-foot segment and the rigid foot were

similar to each other, leading to the closeness of the respective ankle powers. The results of comparison between methods to calculate ankle work showed that the difference in between the two methods were statistically significant (p-value 0.0004). The difference, though, was not clinically significant as observed in the ankle power graphs. The mean estimate of the difference was only 1.5 J, which could be considered negligible in comparison to the actual work estimate at ~ 59 J.

The rigid foot model only slightly underestimated the ankle work as compared to the multi-segment foot model. This result was unexpected since most walking studies have shown that the rigid foot model actually overestimated ankle power. Bruening et al. (2012b) used sagittal planes to define anatomical reference frames of the foot segments. The rigid foot model in their study used markers that were analogous to AJC, MT2 and MTP joints defined in Table 1 and Table 2. The addition of the mid-tarsal and metatarsophalangeal joint kinetics led to the decrease in peak ankle power being generated at late stance. A similar result was also obtained by MacWilliams et al. (2003). Contrasting results between these walking studies and the current standing vertical jumping study, as well as the close proximity of the ankle power using rigid foot and multi-segment foot models encouraged investigating a change in definition of markers for the rear-foot.

Ankle power graphs obtained in Figure 12 after the change in definitions of rear-foot suggested that ankle power may be over-estimated by the rigid foot model, which is in agreement with what is seen in gait studies shown in Figure 2 (Bruening et al., 2012b). The change that was done considered calcaneus, navicular and cuboid markers to define the anatomical reference frame of the rear-foot. The change effectively meant that the rear-foot was considered as all hind-foot and a massless mid-foot. The moments and forces at the MTP joints and the mid-tarsal joint would then be equal and opposite to each other with respect to the mid-foot. Essentially, this way of

obtaining ankle power would be analogous to the power obtained using a three-segment foot with a massless mid-foot. These results also re-emphasize that the rear-foot is in fact not a single rigid segment. If the rear-foot were rigid, changing the marker set should not have meaningfully affected the ankle power results for the multi-segment model.

Analogous to the change of markers defining the anatomical reference frame of the rear-foot done in this study, Zelik et al. (2018) also used a slight modification of distal foot power to obtain distal calcaneus power. Their results indicated that distal calcaneus power included a phase of power generation greater than and a phase of power absorption smaller than distal foot power, and that ankle power was overestimated by distal foot power technique. These observations suggested that the hind-foot or calcaneus is more rigid than other distal segments of the foot. Similar to Zelik et al. (2018) study, when the current study considered the rear-foot as all hind-foot and a massless mid-foot, the ankle power computed from the multi-segment foot model decreased, whereas ankle power due to rigid foot remained almost similar. Both these results suggest the foot contains rigid calcaneus (or hind-foot) and other non-rigid segments, which in essence, emphasize the non-rigid nature of the foot.

5.3   Limitations and Future Work:

It is evident from past studies as well as this study that care should be taken while modeling the foot as a rigid body. Due to the absence of literature available for different methods of foot power in the standing vertical jump, it was challenging to be able to compare and validate the foot power results directly. Consistent with the results from the current study, results in walking, running, and running jumps also showed that power and work inside the foot were significant. However, there were no meaningful differences between ankle power results between rigid foot model and two-segment foot model. The ankle power results obtained after the change in

definitions of the rear-foot suggest that a model with three (or more) segments could provide more insight into ankle kinetics. The current method used for studying the two-segment foot using adjacent force platforms would be impractical to study a three-segment foot. Therefore, future studies could consider modeling the rear-foot using markers from the hind-foot as a proxy for using a three-segment model. The three-segment foot study as proposed could help better understand the effects of foot power on ankle kinetics.

The current study was implemented to focus on foot and ankle energetics on the right leg. Future research protocols could focus on the knee and hip joints as well as pelvis and consider including the study of the contralateral leg as well. Such a study could help evaluate power flows in both lower leg extremities simultaneously and better understand the role of foot power on the other joints and segments. A full bilateral lower limb model along with multi-segment foot could also expand our understanding of the dominant limb effect.

The definition of the fore-foot segment and the MTP joints in this study involved simplifying assumptions. The fore-foot was considered as a uniform elliptical cylinder and the MTP joints were assumed to be acting at the joint space between second and third metatarsal head. However, the toes have gaps in between them and are not the same size. This was compensated by assuming uniform density, but a better model for the forefoot could provide more accuracy.

Another limitation of the study was the sample size. The study was done with three men and three women participants of similar young age group. Hence, the results that were obtained are not be representative of all populations.

6   Conclusion:

With the underlying assumption of a rigid body model, studying foot mechanics is relatively simple, but essentially flawed. This is because the foot is not a rigid body, owing to the various joints, as well as soft tissue deformations internal to the foot. It is likely that inter-foot joints and periarticular soft tissues make important contributions to energy flows in standing vertical jump, a jump important in sports such as volleyball and basketball. To assess jumping performance and to maximize it, it is imperative to study the non-rigid nature of the foot. Three methods that evaluated different aspects of the internal foot power: distal foot power, foot power imbalance, and MTP power were compared, and statistically significant differences were observed between all three methods. Two methods that evaluated ankle power using rigid and multi-segment model of the foot showed no clinically significant differences. A change in markers defining the rear-foot to entirely hind-foot markers caused a significant difference between ankle power using rigid and modified multi-segment foot model.

The results suggested that foot power imbalance encompasses power contributions from all areas of the foot, whereas distal foot power only includes contribution due to the motion of the center of pressure relative to the foot center of mass, and that MTP joints are only one such source of foot power. In order to quantify the power flows internal to the foot, either distal foot power or power balance technique could be used given that the limitations of the method being used are properly understood. Results of ankle power suggested that modeling the foot as two rigid segments does not incorporate the actual non-rigid nature of the foot. A better multi-segment foot model would be imperative to achieve improved understanding.

Results of the study encourage further research to compare the distal foot power and power balance techniques, as well as developing better strategies than the adjacent force platform

method to study kinetics of a three-segment foot model. Future studies aimed at maximizing

jumping performance could account for the non-rigid nature of the foot in specifying different

jump parameters and outcomes. These further explorations would result in a more complete

accounting of foot kinetics and how they affect kinetics of the ankle and other proximal joints as

well as how they influence performance outcomes.

7   References:

Ackland, T.R., Henson, P.W., Bailey, D.A., 1988. The Uniform Density Assumption: Its Effect upon the Estimation of Body Segment Inertial Parameters. International Journal of Sport Biomechanics 4, 146–155. https://doi.org/10.1123/ijsb.4.2.146

Aragón-Vargas, L.F., Gross, M.M., 1997. Kinesiological Factors in Vertical Jump Performance: Differences among Individuals. Journal of Applied Biomechanics, 13(1), 24-44.

Bezodis, N.E., Salo, A.I.T., Trewartha, G., 2012. Modeling the Stance Leg in Two-Dimensional Analyses of Sprinting: Inclusion of the MTP Joint Affects Joint Kinetics. Journal of Applied Biomechanics 28, 222-227.

Bruening, D.A., Cooney, K.M., Buczek, F.L., Richards, J.G., 2010. Measured and estimated ground reaction forces for multi-segment foot models. Journal of Biomechanics 43, 3222–3226. https://doi.org/10.1016/j.jbiomech.2010.08.003

Bruening, D.A., Cooney, K.M., Buczek, F.L., 2012a. Analysis of a kinetic multi-segment foot model. Part I: Model repeatability and kinematic validity. Gait & Posture 35, 529–534. https://doi.org/10.1016/j.gaitpost.2011.10.363

Bruening, D.A., Cooney, K.M., Buczek, F.L., 2012b. Analysis of a kinetic multi-segment foot model part II: Kinetics and clinical implications. Gait & Posture 35, 535–540. https://doi.org/10.1016/j.gaitpost.2011.11.012

Bruening, D.A., Takahashi, K.Z., 2018. Partitioning ground reaction forces for multi-segment

    foot joint kinetics. Gait & Posture 62, 111–116.

    https://doi.org/10.1016/j.gaitpost.2018.03.001

Buczek, F.L., Kepple, T.M., Siegel, K.L., Stanhope, S.J., 1994. Translational and rotational joint

    power terms in a six degree-of-freedom model of the normal ankle complex. Journal of

    Biomechanics 27, 1447–1457. https://doi.org/10.1016/0021-9290(94)90194-5

Carson, M.C., Harrington, M.E., Thompson, N., O'Connor, J.J., Theologis, T.N., 2001.

    Kinematic analysis of a multi-segment foot model for research and clinical applications: a

    repeatability analysis. Journal of Biomechanics 34, 1299–1307.

    https://doi.org/10.1016/S0021-9290(01)00101-4

Cowley, M.S., MacWilliams, B.A., Armstrong, P.F., 2001. A multi-segment kinematic and

    kinetic foot model for clinical decision making. Gait and Posture 13, 297.

Dixon, P.C., Böhm, H., Döderlein, L., 2012. Ankle and midfoot kinetics during normal gait: A

    multi-segment approach. Journal of Biomechanics 45, 1011–1016.

    https://doi.org/10.1016/j.jbiomech.2012.01.001

Leardini, A., Benedetti, M.G., Catani, F., Simoncini, L., Giannini, S., 1999. An anatomically based protocol for the description of foot segment kinematics during gait. Clinical Biomechanics 14, 528–536. https://doi.org/10.1016/S0268-0033(99)00008-X

MacWilliams, B.A., Cowley, M., Nicholson, D.E., 2003. Foot kinematics and kinetics during adolescent gait. Gait & Posture 17, 214–224. https://doi.org/10.1016/S0966-6362(02)00103-0

McGibbon, C.A., Krebs, D.E., 1998. The influence of segment endpoint kinematics on segmental power calculations. Gait & Posture 7, 237–242. https://doi.org/10.1016/S0966-6362(97)00041-6

Nagano, A., Ishige, Y., Fukashiro, S., 1998. Comparison of new approaches to estimate mechanical output of individual joints in vertical jumps. Journal of Biomechanics 31, 951–955. https://doi.org/10.1016/S0021-9290(98)00094-3

Robertson, D.G., Winter, D.A., 1980. Mechanical energy generation, absorption and transfer amongst segments during walking. Journal of Biomechanics 13, 845–854.

Robertson, D.G., Fleming, R.D., 1987. Kinetics of standing broad and vertical jumping. Canadian Journal of Applied Sport Sciences 12. 19-23.

Siegel, K.L., Kepple, T.M., Caldwell, G.E., 1996. Improved agreement of foot segmental power and rate of energy change during gait: Inclusion of distal power terms and use of three-dimensional models. Journal of Biomechanics 29, 823–827. https://doi.org/10.1016/0021-9290(96)83336-7

Stefanyshyn, D.J., Nigg, B.M., 1998. Contribution of the lower extremity joints to mechanical energy in running vertical jumps and running long jumps. Journal of Sports Sciences 16, 177–186. https://doi.org/10.1080/026404198366885

Takahashi, K.Z., Kepple, T.M., Stanhope, S.J., 2012. A unified deformable (UD) segment model for quantifying total power of anatomical and prosthetic below-knee structures during stance in gait. Journal of Biomechanics 45, 2662–2667. https://doi.org/10.1016/j.jbiomech.2012.08.017

Takahashi, K.Z., Stanhope, S.J., 2013. Mechanical energy profiles of the combined ankle–foot system in normal gait: Insights for prosthetic designs. Gait & Posture 38, 818–823. https://doi.org/10.1016/j.gaitpost.2013.04.002

Vanezis, A., Lees, A., 2005. A biomechanical analysis of good and poor performers of the vertical jump. Ergonomics 48(11-14), 1594-1603. https://doi.org/10.1080/00140130500101262

Vanrenterghem, J., Lees, A., Lenoir, M., Aerts, P., De Clercq, D., 2004. Performing the vertical jump: Movement adaptations for submaximal jumping. Human Movement Science 22, 713–727. https://doi.org/10.1016/j.humov.2003.11.001

Winter, D.A., 1996. Total Body Kinetics: Our Diagnostic Key to Human Movement. ISBS - Conference Proceedings Archive 1.

Winter, D.A., 2009. Biomechanics and Motor Control of Human Movement. John Wiley & Sons, Waterloo, Ontario, Canada.

Yu, B., Gabriel, D., Noble, L., An, K., 1999. Estimate of the Optimum Cutoff frequency for the Butterworth Low-Pass Digital Filter. Journal of Applied Biomechanics 15, 318-329. https://doi.org/10.1123/jab.15.3.318

Zelik, K.E., Takahashi, K.Z., Sawicki, G.S., 2015. Six degree-of-freedom analysis of hip, knee, ankle and foot provides updated understanding of biomechanical work during human walking. Journal of Experimental Biology 218, 876–886. https://doi.org/10.1242/jeb.115451

Zelik, K.E., Honert, E.C., 2018. Ankle and foot power in gait analysis: Implications for science, technology and clinical assessment. Journal of Biomechanics 75, 1–12. https://doi.org/10.1016/j.jbiomech.2018.04.017